BAU Journal - Health and Wellbeing

Volume 4 | Issue 1
ISSN: 2617-1635

Article 9

October 2021

DZ-BAU2021-14N AS NOVEL PYRAZOLOPYRIDINE NANOCRYSTALS: APPRAISAL OF ANTICANCER ACTIVITY AGAINST HCT-116 AND HT-29 COLORECTAL CANCER CELL LINES

Zahra Kassem
Lab Technician in Research Pharmaceutical Technology Lab, Pharmaceutical Sciences Department, Faculty of Pharmacy, Beirut Arab University, Beirut, Lebanon, zahra.kassem@bau.edu.lb

Soumaiah Abou Staiteieh
Genomic Surveillance and Biotherapy (GSBT) Laboratory, Biology Department, Faculty of Sciences, R. Hariri Campus, Lebanese University, Hadath, Lebanon, somaia_30_6@hotmail.com

Jamal Nasr
Genomic Surveillance and Biotherapy (GSBT) Laboratory, Biology Department, Faculty of Sciences, R. Hariri Campus, Lebanese University, Hadath, Lebanon, jamalnasr1@hotmail.com

Amina Mneimneh
Postgraduate Student, Faculty of Pharmacy, Beirut Arab University, Beirut, Lebanon, a.mneimneh@bau.edu.lb

Ali Youssef
Research Associate, Faculty of Arts and Sciences, American University of Beirut, Beirut, Lebanon, ali.youssef@gmail.com

DZ-BAU2021-14N AS NOVEL PYRAZOLOPYRIDINE NANOCRYSTALS: APPRAISAL OF ANTICANCER ACTIVITY AGAINST HCT-116 AND HT-29 COLORECTAL CANCER CELL LINES

Abstract

Mentioning DZ-BAU2021-14 ($C_{19}H_{17}N_5O_2$,347.370 g/mol) developed in BAU Labs, its promising preliminary antitumor effect nominated it to be selected as a lead antiproliferative compound against colorectal cancer cell lines owing to its proved Cyclin Dependent Kinase 2 (CDK2) inhibition (Kassem *et al.*, 2021). Solving many problems restricting traditional cancer therapy, nanotechnology is offering safety margins and targeted delivery of poorly soluble drug. The potential effect of this compound was combined with the advantages of nanotechnology, precisely nanocrystals to achieve better antiproliferative and hopeful less cytotoxic patterns. The nanocrystals DZ-BAU2021-14N were prepared by an antisolvent precipitation technique using Poloxamer 407 and Cremophor® RH 40 as stabilizers. The nanocrystals were obtained with a nanometric particle size (89.80 ± 11.2 nm) and a negative zeta potential (-32.6 ± 0.50 mV) and were stable at 4 ± 0.5°C with no significant change in particle size or zeta potential. The anticancer activity of DZ-BAU2021-14 and DZ-BAU2021-14N were assessed. Their antiproliferative effects against colorectal cancer cell lines HCT-116 and HT-29 were studied via viability assay. In addition, their cytotoxic effects on non-tumorigenic cell lines NCM-460D were evaluated and respective IC50 values were determined. Different responses were obtained; DZ-BAU2021-14N provided lower IC50 on HCT-116 compared to the free drug DZ-BAU2021-14 (27 and 22 µM, respectively). The safety profile of the free drug was reflected by its IC50 on NCM-460D of 200µM while that of drug nanocrystals showed relative cytotoxicity with IC50 of 33µM, and this requires further investigation to study this response.

Keywords

Pyrazolopyridine, Nanocrystals, Colorectal cancer, Antiproliferative, HCT-116, HT-29, NCM-460D

Authors

Zahra Kassem, Soumaiah Abou Staiteieh, Jamal Nasr, Amina Mneimneh, Ali Youssef, Nadine Darwiche, Doaa Issa, Raghida Bou Merhi, and Mohammed Mehanna

1. INTRODUCTION

Cancer is considered nowadays, a global health threat. It is the world's second leading cause of death, and is predicted in the coming years to be the main cause of death (Siegel *et al.*, 2019). Cancer is a disease involving abnormal and uncontrolled cell growth. There are many types of cancer each with own set of symptoms (Kumar Shital, 2021). Despite the disease's malignancy, it is still possible to lower mortality rates, before invasion and progression to metastasis, by early and accurate diagnosis and treatment.

In spite of the requisite advancements occurring in design and production of various anticancer agents over the last decades, existing and accessible therapies still have two major drawbacks; the lack of selectivity and targeted delivery for cancer tissues causing undesirable side effects, and the development of drug resistance by cancer cells making them unresponsive to standard therapy which is considered one of the most pressing dilemmas in cancer therapy (Alfarouk *et al.*, 2015; Pick *et al.*, 2010). The absence of perfect anticancer therapies necessitates new approaches to improve quality of current treatments. As a result, the principle of developing targeted drugs arises as solution to this global problem (Fares *et al.*, 2020).

Colorectal Cancer (CRC) is being primarily localized within the colon and rectum (Stintzing *et al.*, 2017). The annual report in United States studying the prevalence of different types of cancer was stating that colorectal cancer (CRC) is the third most common cancer among women and men (Jemal *et al.*, 2017). Additionally, CRC is the fourth leading cause of cancer mortality in both men and women. CRC occurs chiefly in populations over 50 years of age though it can happen at any age and annual deaths around 690,000 people (Rejhová *et al.*, 2018). More than half of CRC cases worldwide are registered in developed countries, with rising incidences in developing ones (Kuipers *et al.*, 2015). The current treatment of CRC is based on surgery and chemotherapy. Taxol, 5-Fluorouracil (5-FU), Doxorubicin and Roscovitine, are used to treat human colorectal cancer individually and/or in combination (Abaza et al., 2008).

Roscovitine, 2-(R)-(1-ethyl-2-hydroxyethylamino)-6-benzylamino-9-isopropylpurine (Fig. 1), belongs to purines family which has an imidazopyrimidine structure. Roscovitine arrests the cell cycle in G0, G1, S or G2/M, by directly inhibiting Cyclin Dependent Kinases (CDKs) (Cicenas *et al.*, 2015). It showed antiproliferative effect on CRC cell lines HCT-116 and HT-29 with IC50 value of 12.24 and 14.6 µM respectively (McClue *et al.*, 2002; Taha *et al.*, 2020).

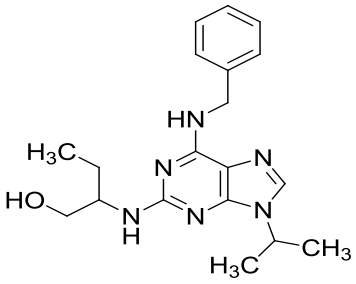

Roscovitine
HCT-116 IC50 = 12.24 µM
Taha *et al.*, 2020
HT-29 IC50 = 14.60 µM
McClue *et al.*, 2002

Fig.1: Antiproliferative effect of Roscovitine on HCT-116 and HT-29

Pyrazolopyrimidine and pyrazolopyridine are considered isosteric analogs to imidazopyrimidine, they possess a wide variety of biological activities. They were highlighted being antimicrobial (Abdelmohsen & El Emary, 2014), antimalarial (Pinheiro *et al.*, 2019), antitumor (Karrouchi *et al.*, 2018), tuberculostatic (Hu *et al.*, 2019), anti-inflammatory agents (Dennis Bilavendran *et al.*, 2020) and having cardiovascular activities (Avari, 2019). They also demonstrated antiproliferative effect on colorectal cancer cell lines (Fig. 2). Synthesizing pyrazolo[3,4-d]pyrimidines as anticancer agents, compound 2-((4-(benzylamino)-1*H*-pyrazolo[3,4-d]pyrimidin-6-yl)amino)ethan-1-ol (1) showed high activity on colorectal cancer cell line HCT-116 with IC50 value of 4.5 µM (Ismail *et al.*, 2016). 5,7-Dihydroxy-2-((4-methoxyphenyl)amino)-N-phenylpyrazolo[1,5-a]pyrimidine-3-carboxamide) (2) showed antitumor activity against colorectal cancer cells HCT-116 exhibiting IC50 of 58.44 ± 3.8% µg/mL equivalent to 149 ± 3.8% µM (Hassan *et al.*, 2017).

Pyrazolopyridopyrimidine analogs, designed and synthesized as hybrid scaffolds for their antimicrobial and antitumor potential, deliberated the promising 5-imino-3-methyl-4-phenyl-1,4,5,9-tetrahydro-6*H*-pyrazolo[4',3':5,6]pyrido[2,3-d]pyrimidin-6-amine (3) being the most active compound against HCT-116 cell line with an IC50 value of 3.18 µM (El-Gohary *et al.*, 2019). In attempts to design and synthesize antitumor agents with improved solubility and pharmacokinetic properties, 3-(4-(methoxymethyl)-1*H*-benzo[d]imidazol-2-yl)-5-(pyridin-3-yl)-1*H*-pyrazolo[3,4-b]pyridine (4), exerted significant activity against HCT-116 IC50 = 0.019 µM (Fig. 2) (Lin *et al.*, 2007).

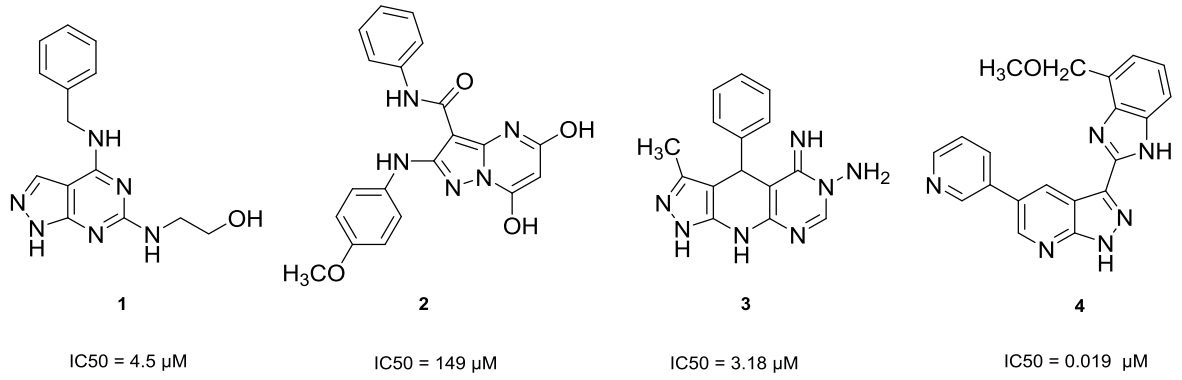

Fig.2: Structures and IC50 of some pyrazolo-pyrimidine and -pyridine derivatives on HCT-116 cancer cell line

Nanotechnology has been proved to solve some of the main problems limiting conventional cancer treatments, it might offer more specific delivery of therapeutics and reduction of toxic secondary effects. It plays a significant role in targeted delivery and release of drugs such as nanoparticles, dendrimers, nanoshells, liposomes, niosomes, nanocrystals, and magnetic nanoparticles (Alexis *et al.*, 2008; Rajendra *et al.*, 2018). Recently nanocrystalization technology has sparked a lot of interest as a way to overcome the obstacles of poorly soluble anticancer drugs. These nanocrystals (NSs) are colloidal dispersions of pure drug in an outer liquid phase with particle size ranging from 100 to 1,000 nm with a large surface area to enhance solubility and bioavailability of these drugs (Mohyeldin *et al.*, 2016).

Mainly there are two main techniques to produce NCs; the top-down method which is based on size reduction of the large particles into smaller ones, and the bottom-up technologies that depend on the growth of small particles from individual molecules as in the antisolvent precipitation process (de Waard *et al.*, 2011). The latter is a popular approach used for its simplicity and low setup cost (Freag *et al.*, 2013; Saindane *et al.*, 2013; Tian *et al.*, 2013).

Understanding the problems of available anticancer drugs, the role of nanocrystalization, in potentiating the efficacy of a new molecule, is a target.

In consequence, this study mainly aims to construct DZ-BAU2021-14N nanocrystals utilizing the antisolvent precipitation technique with the aid of two different stabilizers, and to evaluate its *in-vitro* antiproliferative and cytotoxic effect in comparison to free DZ-BAU2021-14 using MTT assay on two colorectal cancer cell lines HCT-116 and HT-29 compared to non-tumorigenic NCM-460D. Establishing the average particle size and zeta potential of the prepared nanocrystals as well as evaluating the interaction between the molecule under investigation and the polymers in the nanopreparation using Fourier transform infrared spectroscopy (FT-IR) and X-ray diffraction (XRD) technique are considered as fundamental objectives the current study.

2. MATERIALS AND METHODS

2.1. Nanocrystal's Formulation

2.1.1.Materials

DZ-BAU2021-14 was synthesized in BAU Labs, Poloxamer 407 and Cremophor® RH 40 were purchased from Sigma-Aldrich Co. (St Louis, MO, USA). All organic solvents were of analytical grade and purchased from Sigma-Aldrich.

2.1.2. Screening stabilizers for the nanoprecipitation technique

The previous selection for the optimal stabilizer was based on the ability of these different stabilizers to achieve stable nanocrystals and was applied as a screening parameter (Mohyeldin *et al.*, 2016). Poloxamer® 407 and Cremophor® RH40 were used with 0.5% w/v and 1% w/v, respectively. The selection was based on the average particle size and the Polydispersity Index (PDI) of the formed nanocrystals.

2.1.3. Preparation of the nanocrystals

DZ-BAU2021-14 nanocrystals were tailored by applying the antisolvent nanoprecipitation technique previously reported (Mohyeldin *et al.*, 2016). Briefly, a saturated solution of the molecules under investigation dissolved in acetone was added to deionized water as the non-solvent phase, containing a suitable stabilizer at a ratio of 1:10. The solvent phase was added to the aqueous phase with rapid stirring at room temperature (25 ± 0.5°C) for 30 minutes.

2.1.4. Particle characteristics

2.1.4.1. Physicochemical characteristics of DZ-BAU2021-14N nanocrystals

Droplet size, zeta potential, and PDI were measured at 25 ± 2°C and 90° scattering angle by Zeta sizer 2000 (Malvern Instruments, UK) after dilution with deionized water (1:100 v/v) (Zhou *et al.*, 2018). All measurements were carried out in triplicate and mean ±SD was calculated.

2.1.4.2. Fourier transform infrared spectroscopy (FT-IR)

To assess whether there is any possible interaction between the free drug, Poloxamer 407, Cremophor® RH 40, their physical mixture, and the prepared nanocrystals (after freeze-drying) an FT-IR spectrometer (PerkinElmer Inc., Waltham, MA USA) was used. Each sample was mixed with dry infrared (IR) grade of crystalline potassium bromide then compressed at 10 tons in a hydraulic press to form a thin disk. Each sample was scanned within the spectral region of 4,000 and 400 cm^{-1} with a resolution of 4 cm^{-1} (Aguayo *et al.*, 2018).

2.1.4.3. X-ray diffraction (XRD)

All samples were analyzed using a Siemens D-500 X-ray powder diffraction (XRD) device. CuKα was targeted using a voltage of 40 kV and a current of 30 mA during the XRD measurements and circumstances. A modified system of diverging and receiving as well as receiving and anti-scattering slits of 1°, 1°, 1°, and 0.15°, respectively, was utilized. Jade 6.0 (Materials Delta Inc.) was used for data processing. The XRD patterns were obtained using a step width of roughly 0.04° 2θ between 5° and 50° (Kaviyarasu *et al.*, 2017).

2.1.4.4. Storage stability

The physical and thermal stability was assessed by performing short-term storage studies. The formulated nanocrystals were stored in capped amber glass vials at two different temperatures (4°C and 25°C as the refrigerator and room temperature, respectively) for 3 months. Every month, the stored formulations were monitored by droplet size, zeta potential, PDI determination (Mehanna *et al.*, 2020).

2.2. In-Vitro Cytotoxicity Study

2.2.1. Cell lines

Two colorectal cancer cell lines HCT-116 and HT-29 in addition to normal one NCM-460D were chosen for testing antiproliferative effect and cytotoxicity. HCT-116 (ATCC-CCL-247) are adherent epithelial cells derived from colorectal cancer in an adult male; having a mutation at codon 13 of the proto-oncogene RAS. HT-29 (ATCC-HTB-38) are adherent epithelial cells derived from colorectal cancer from a 44-year-old

adult Caucasian female; having a mutation at codon 273 of the p53 gene. NCM-460D (INCELL-2016) are normal adherent epithelial cells derived from the colon mucosa of a 68-year-old Hispanic male and used as a control.

2.2.2. Antiproliferative and cytotoxic evaluation

To evaluate the antineoplastic effect and safety of the formulation, the antiproliferative effect and cytotoxicity of the DZ-BAU2021-14N nanocrystals, as well as free drug, were assessed using 3(4,5-dimethylthiazol-2-yl)-2,5-diphenyltetrazolium bromide (MTT) assay on colorectal cancer cell lines HCT-116 and HT-29 in addition to normal one NCM-460D.

2.2.3.Medium and cell culture

The cancerous cell lines HCT-116, HT-29 were seeded in Dulbecco's Modified Eagle Medium (DMEM) supplemented with 10% heat-inactivated fetal bovine serum (FBS) (Sigma), 1% penicillin and streptomycin (Sigma). NCM-460D non-tumorigenic cell lines were seeded in M3:BaseF^{TM} culture medium (INCELL) supplemented with 10% heat-inactivated fetal bovine serum (FBS) (Sigma), 1% penicillin and streptomycin (Sigma).

2.2.4. Cell viability treatment and testing

The culture of cell lines was carried out in flasks of 75 cm^2. When the confluence reaches approximately 80%, the passage by trypsinization was carried out. Cells were washed with PBS-1X and then 2 ml of 1X trypsin (Lonza) were added. The cells were then incubated for 5 minutes at 37˚C to allow complete detachment. Suitable complete medium for each line was added to stop the action of trypsin. After centrifugation for 5 minutes at 1000 rpm, cells were resuspended in an appropriate medium (table 1), diluted according to a specific factor, and then transferred to flasks containing 10 ml of the medium. The cells were incubated at 37˚C and 5% CO_2, so that they reach confluence at 72 hours and were ready to use.

2.2.4.1. Cell counting

The Neubauer chamber was used to calculate the concentration of cells in a suspension. Each counting area was made up of 9 squares (0.1 cm × 0.1 cm) and covered with a glass slide 0.01 cm above the surface of counting area. After detaching the Cells by trypsinization and centrifugation for 5 minutes at 1000 rpm, cells were suspended in corresponding medium. An equivalent volume of cells and trypan blue were mixed and an aliquot was placed in the hemocytometer. The total number of cells was determined by dividing total number of white cells × 10000) by (number of squares counted × dilution).

2.2.4.2. Preparation of study compounds

Initial 12.5 mM solutions of test compound and its nanocrystals were prepared; DZ-BAU2021-14 in DMSO and stored at -20ºC, while DZ-BAU2021-14N in water and stored at 8ºC. Water was used to prepare intermediate solutions of 1 mM concentration according to the formula C1 V1 = C2 V2, and used to prepare the concentration range (10 µM, 20 µM, 40 µM and 50 µM) according to the same formula.

2.2.4.3. Treatment and viability assay

The MTT test was performed to study the antiproliferative effect of compounds. This colorimetric method is based on reduction of “yellow tetrazolium dye” 3-(4,5-dimethylthiazol-2-yl)-2,5-diphenyltetrazolium bromide (MTT) to blue-violet formazan crystals by metabolically active cell (Fig. 3). The amount of formazan produced is therefore proportional to the metabolic activity of viable cells and results were expressed as a percentage of viability compared to the controls treated with DMSO alone.

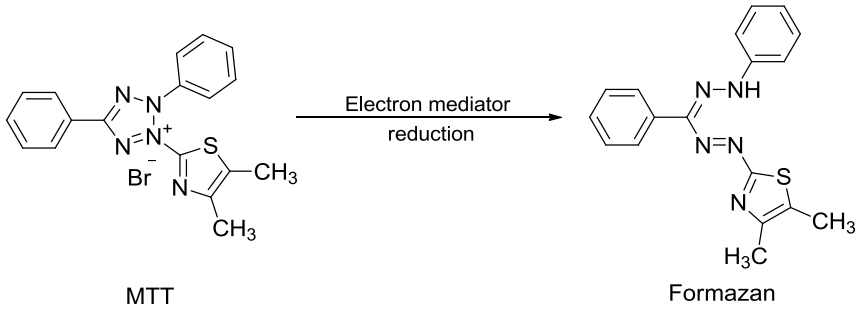

Fig.3: Metabolic conversion of MTT to formazan by viable cells

After trypsinization, cells were counted, cultured, at a specific number and in a suitable medium (Table 1), in 96-wells plates and incubated for 24 hours before their treatment, at 37°C and 5% CO_2, so that they adhere and their confluence reaches 60%.

Table 1: Number of cells seeded per well and the corresponding medium.

Cell line	Number of cells per well	Culture environment
NCM-460D	12000	M3:Base^{FTM}
HCT-116	7000	DMEM
HT-29	7000	DMEM

Cells were treated with different concentrations of DZ-BAU2021-14 and DZ-BAU2021-14N (10 µM, 20 µM, 40 µM and 50 µM). A concentration of 0.4% DMSO was used in DZ-BAU2021-14 experiments after guaranteeing 100% viability of cell lines with this concentration. After adding 10 µl of the MTT solution (5 g/L) (Sigma-Aldrich) to each well followed by a 3-hour incubation, the formed purple crystals were dissolved in 100 µl of stop solution (SDS 10% and HCl 1N) and left overnight. The color was then quantified using colorimetric assay by photon absorption spectrometry at a wavelength of 595nm (ELISA Reader, multi-well scanning spectrophotometer). The MTT test was done at 24, 48 and 72 hours after cells treatment. Three to four trials of each experiment were affected and an average response was admitted. Dose response curves were plotted, graphs, Standard Deviation (SD) and Standard Error (±SE) were created and calculated using Microsoft Excel software (2016 edition). Using GraphPad Prism 8 Software (San Diego, CA, USA), statistical significance comparing the treatment conditions with their controls was analyzed by two-way ANOVA with Dunnett's multiple comparisons test.

2.2.4.4. Determination of the concentration inhibiting 50% of proliferation (IC50)

IC50 values were calculated using GraphPad Prism 8 software after transforming the concentrations of compounds into log values and normalized the values of the effect of each concentration with 0% defined as the smallest mean in each data set and 100% defined as the largest mean in each data set. Statistical significance comparing treatment conditions between DZ-BAU2021-14 and DZ-BAU2021-14N was analyzed by one-way ANOVA with Sidak's multiple comparisons test. A confidence level of $P < 0.05$ was considered statistically significant.

3. RESULTS AND DISCUSSION

The promising antineoplastic pattern of DZ-BAU2021-14 against colorectal cancer cell lines HCT-116 and HT-29, and its minor cytotoxicity on non-tumorigenic NCM-460D (Kassem *et al.*, 2021), in addition to the significant role of nanocrystals in enhancing the efficacy of many drugs

directed the authors of the current study to extrapolate their anticipations to achieve better antiproliferative effects and cytotoxicity margins getting benefit of the lead DZ-BAU2021-14 involving it in a nanocrystalline system. DZ-BAU2021-14 was reported to reveal low order of lipophilicity; 2.90-3.43 as estimated n-octanol/water partition coefficients and 3.16 Log $P_{o/w}$, expecting optimal lipophilic behavior and poor to moderate water solubility (Kassem *et al.*, 2020). This finding likewise encouraged the authors of this work to improve the physical properties of DZ-BAU2021-14 trying to enhance its poor water solubility.

3.1. Particle Characteristics

3.1.1.Effect of the stabilizer concentration

It was important to study the stabilizer concentration effect on nanocrystals characteristics. This was assessed by particle size, polydispersity index, and zeta potential. Using each stabilizer alone resulted in large particles with sizes 852 ± 134.15 and 1229 ± 308.72 nm for Poloxamer and Cremophor respectively. However, using different ratios of Poloxamer: Cremophor (PLX : CRM) returned in different effects on particle size; using PLX : CRM ratio 1:1 resulted in remarkable particle size reduction compared to each stabilizer alone. On the other hand, PLX: CRM ratios of 1:2 and 2:1 didn't show advantage in particle size over the 1:1 ratio (Table 2). The use of Cremophor® RH 40 is essential due to its liability to achieve more stable nanocrystals (Madheswaran *et al.*, 2014). Surfactants with high Hydrophilic-Lipophilic Balance (HLB) are considered good emulsifying ones, stabilizing the aqueous phase and reducing the size of particles (Kamel *et al.*, 2009), hence, addition of the relatively hydrophilic Poloxamer 407 (HLB = 18) to Cremophor® RH 40 affected a reduction in particle size. In the current work, the combination of Poloxamer and Cremophor in 1:1 ratio provided the optimal nanocrystal size with 89.80 ± 11.2 nm, 0.18 ± 0.014, and -32.6 ± 0.50 mv as particle size, polydispersity index and zeta potential respectively (Table 2).

Table 2: Effect of stabilizers ratios on the particle characteristics

Ratio PLX : CRM	Particle size (nm)	polydispersity index (PdI)	Zeta potential (mv)
1:0	852±134.15	0.17± 0.029	-29.76±0.22
0:1	1229±308.72	0.77±0.063	-11.20±0.84
1:1	89.80±11.20	0.18±0.014	- 32.6±0.50
1:2	218±15.73	0.82±0.1	-17.84±0.51
2:1	167± 23.68	0.96±0.08	-27.20±0.30

3.1.2 Crystallinity analysis

XRD patterns for DZ-BAU2021-14, nanocrystals DZ-BAU2021-14N and free nanocrystals are shown in figure 4. DZ-BAU2021-14 showed very strong characteristic diffraction peaks at 2θ of 8.09˚, 8.40˚, 10.30˚, 10.50˚, 12.90˚, 14.15˚, 15.28˚, 17˚, 21.10˚, 24.60˚, 25.90˚ and 27.16˚, indicating the pure crystalline status of the compound (Fig. 4A). The principal peaks of pure DZ-BAU2021-14 were present in freeze-dried mixture DZ-BAU2021-14N but had lower intensity and were shifted down (Fig. 4B). This might be attributed to reduction in particle size.

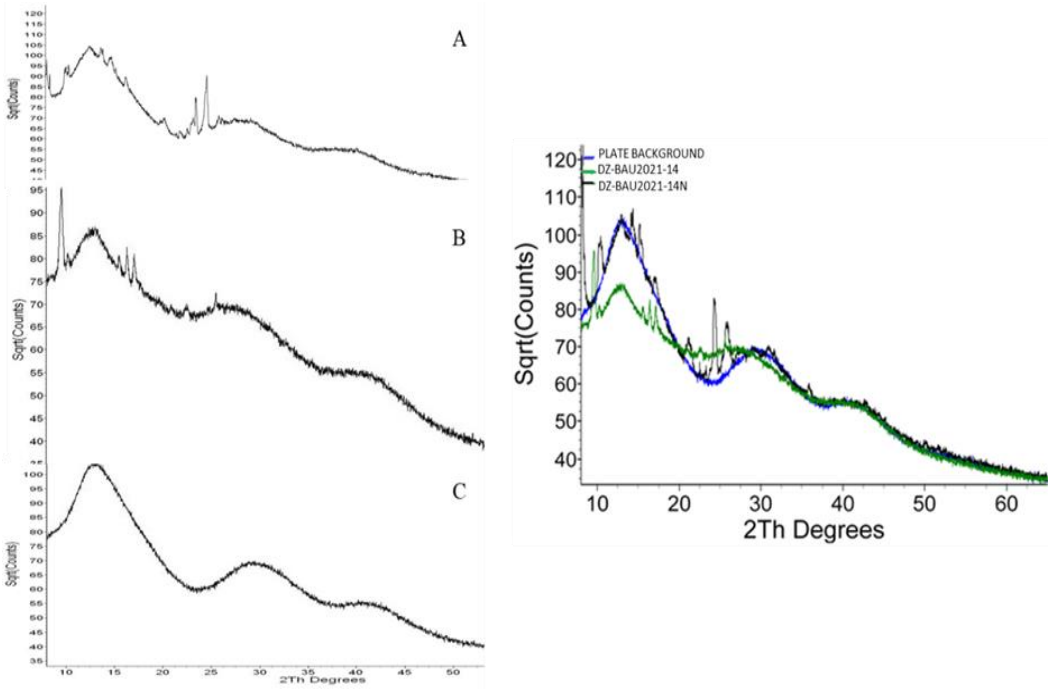

Fig.4: X-ray diffraction (XRD) thermograms of DZ-BAU2021-14 (A), DZ-BAU2021-14N (B) and free nanocrystals (C).

3.1.3. Fourier transform infrared spectroscopy (FT-IR)

IR spectroscopic analysis provides information on chemical bonding, functional groups and presence or absence of changes in the crystalline structure of a compound. FT-IR spectrum of DZ-BAU2021-14 showed distinctive peaks at 3048 cm^{-1} (Aromatic, C-H stretching), 2970 cm^{-1} (C-H stretching), 1712 cm^{-1} (C=O stretching) and C-O-C stretching vibrations at 1066.42 cm^{-1} (Fig. 5A). FT-IR spectra of Poloxamer 407 and Cremophor® RH 40 showed characteristic bands of C-H stretching vibrations at 2883.13 cm^{-1} and 2862.08 cm^{-1}, O-H bending vibrations at 1341.90 cm^{-1} and 1359.42 cm^{-1}, and C-O-C stretching vibrations at 1060.60 cm^{-1} and 1279.38 cm^{-1} (Fig. 5B). In contrast to pure DZ-BAU2021-14, the physical and freeze-dried mixtures showed characteristic C–H stretching vibration bands of Poloxamer 407 and Cremophor® RH 40 in the functional group region at 2859 cm^{-1} and 2921cm^{-1} (Fig. 5(C, D)). There was no change in C–O–O–C bending vibrations in physical and freeze-dried mixtures compared to free nanocrystals nevertheless, a decrease in intensity of the carbonyl stretching at 1712 cm^{-1} was obvious in comparison to the free drug DZ-BAU2021-14 (Fig. 5). This might suggest the presence of hydrogen bonding interactions at the interface between DZ-BAU2021-14 and polymers where a variety of functional groups of different electronic environment provide high opportunities of hydrogen donors-acceptors challenges. The previous findings reflected the chemical stability of the founded nanocrystals.

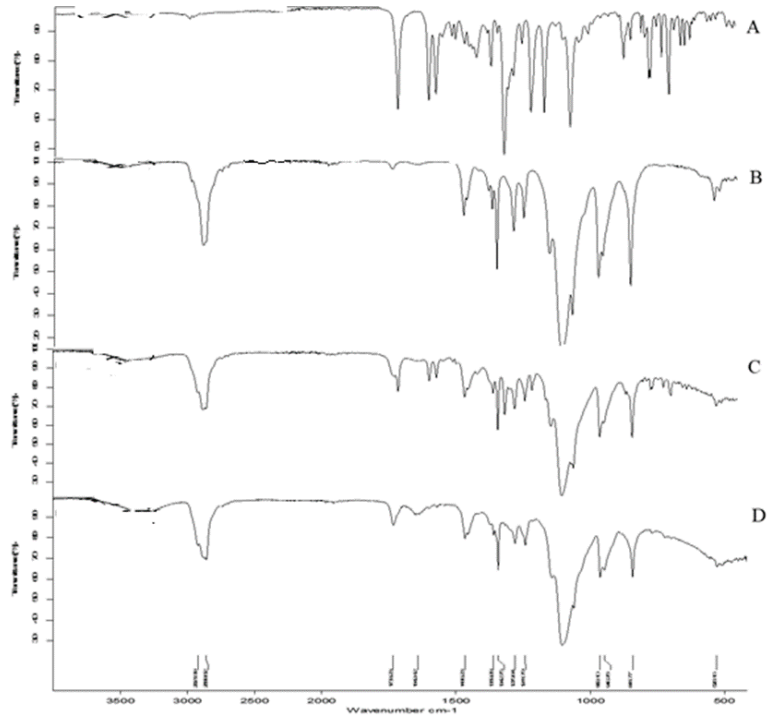

Fig.5: Fourier transform infrared spectroscopy (FT-IR) spectra of DZ-BAU2021-14 (A), free nanocrystals (B), physical mixture (C) and DZ-BAU2021-14N (D).

3.1.4. Stability studies

Formulation stability was assessed determining its physicochemical properties (particle size, PDI, and zeta potential) over the 3 months storage period at room temperature and at 4°C. Nanocrystals revealed no significant change in both particle size and PDI for 3 months at 4°C while particle size increased from 89.80 ± 11.20 to 126.54 ± 13.54 nm after 3 months at room temperature manifesting Ostwald ripening phenomena that is hindered at low temperatures where redisposition of small particles is prevented, while at higher temperature ripening is observed due to fast redisposition of small particles into larger ones.

3.2. In-Vitro Cytotoxicity Study

In the current work DZ-BAU2021-14 and DZ-BAU2021-14N exhibited differential anti-proliferative responses on colorectal cancer cell lines (HCT-116, HT-29) and non-tumorigenic adherent epithelial cell line (NCM-460D). The stabilizers used to prepare nano-crystals were selected having minimal or no cytotoxicity; different types of Poloxamer were tested for their antiproliferative effects on different cancer cell lines and were reported having negligible cytotoxic effects (Subhashni D. Singh-Joy, 2008). Similarly, Cremophor was reported having minor reduction on cell viability in different cancer cell lines (Reinecke et al., 1997).

3.2.1. Antiproliferative effect on HCT-116

DZ-BAU2021-14 showed IC50 values of 27 and 19 µM compared to those of Roscovitine 12.24 and 14.6 µM on colorectal cancer cell lines HCT-116 and HT-29 respectively (Table 3).

Its fifty percent inhibitory concentration was 2-folds higher than that achieved by Roscovitine on HCT-116 cell line and was almost similar to that of Roscovitine on HT-29. The treated colorectal cell lines HT-29, HCT-116 and NCM-460D showed different responses when treated with DZ-BAU2021-14 and DZ-BAU2021-14N (Fig. 6).

Table 3: Percentage proliferation of HCT-116 and HT-29 treated with DZ-BAU2021-14 and DZ-BAU2021-14N

Compound	**HCT-116**									**HT-29**								
	10 µM		**20 µM**		**40 µM**		**50 µM**			**10 µM**		**20 µM**		**40 µM**		**50 µM**		
	48 h	**72 h**	**48 h**	**72 h**	**48 h**	**72 h**	**48 h**	**72 h**	**IC50[2]**	**48h**	**72 h**	**48 h**	**72 h**	**48 h**	**72 h**	**48 h**	**72 h**	**IC50[2]**
DZ-BAU2021-14	74	83	76	84	65	61	58	52	27	80	67	68	53	52	40	48	34	19
St d[1]	17	19	12	9	20	28	14	22		9	7	9	15	3	16	4	10	
DZ-BAU2021-14N	86	71	78	62	62	44	58	42	22	92	83	88	72	88	61	76	83	40
St d[1]	17	19	12	9	20	28	14	22		3	8	12	2	12	5	27	12	
Roscovitine									12.24[3]									14.6[4]

[1]Standard deviations are related to three-four separate experiments, [2]IC50 calculated after 72-hour exposure
[3]Roscovitine reported IC20, IC50 and IC80 = 3.8 ± 0.45, 12.24 ± 1.17 and 39.4 ± 3.16 µM respectively on HCT-116 (Taha et al., 2020)
[4] Roscovitine reported IC50 on HT-29 (McClue et al., 2002)

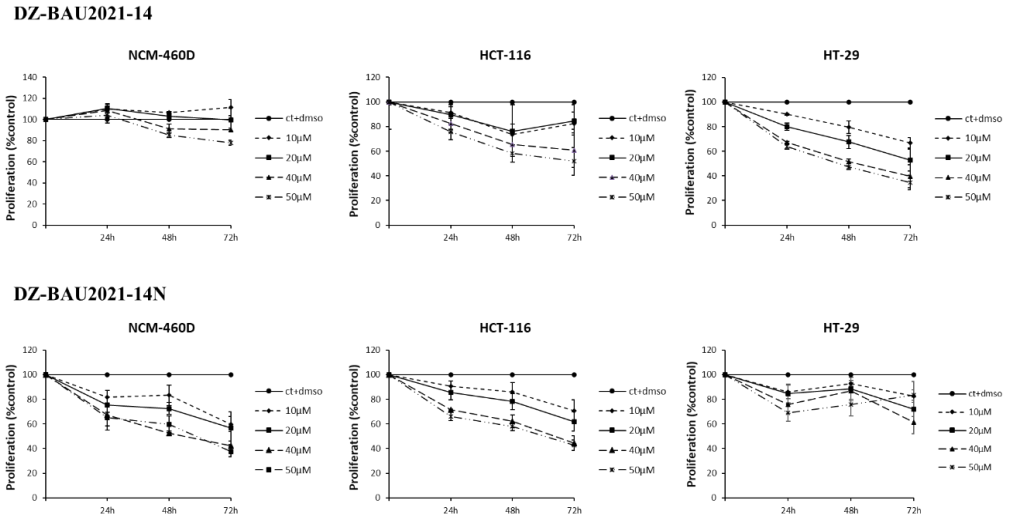

Fig.6: Dose response curves of DZ-BAU2021-14 and DZ-BAU2021-14N against NCM-460D, HCT-116 and HT-29

Percentage proliferation of HCT-116 has been remarkably inhibited in a dose-time dependent manner at 10 µM, 20 µM, 40 µM and 50 µM of DZ-BAU2021-14 after 48h (74 ± 9%, 76 ± 6%, 66 ± 10% and 58 ± 7%) and after 72h (83 ± 9%, 84 ± 5%, 61 ± 14% and 52 ± 11%) respectively (Fig. 7). HCT-116 showed significant sensitivity towards DZ-BAU2021-14N in a dose-time dependent manner at 10 µM, 20 µM, 40 µM and 50 µM at 48h (86 ± 8%, 78 ± 7%, 62 ± 5%, and 58± 3%) and at 72h (71 ± 9%, 62 ± 8%, 45 ± 6% and 42 ± 4%) respectively (Table 3) (Fig. 7). DZ-BAU2021-14N demonstrated superior percentages inhibition on HCT-116 with an IC50 value of 22 µM compared to DZ-BAU2021-14 having IC50 of 27 µM (Table 3) (Fig. 8). This indicates that the fabrication of the DZ-BAU2021-14N nanocrystals enhanced its uptake by this specific HCT-116 cell line.

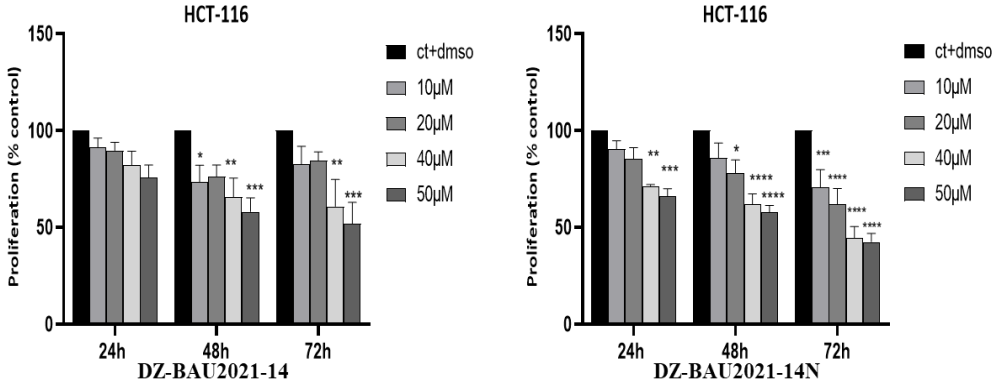

* P<0.05, **0.01<P<0.05, ***P<0.001, ****P<0.0001, P-values were calculated in respect to DMSO

Fig.7: Percentage proliferation of HCT-116 treated with DZ-BAU2021-14 and DZ-BAU2021-14N

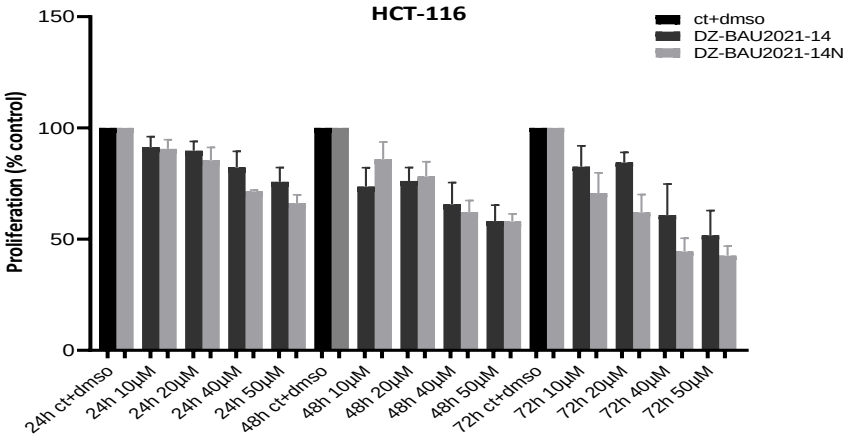

* P<0.05, **0.01<P<0.05, ***P<0.001, ****P<0.0001, P-values were calculated in respect to DZ-BAU2021-14

Fig.8: Comparative antiproliferative effect between DZ-BAU2021-14 and DZ-BAU2021-14N on HCT-116

3.2.2.Antiproliferative effect on HT-29

Figure 6 illustrated higher percentages of growth inhibition assigned to DZ-BAU2021-14 against HT-29 compared to its activity against HCT-116. The percentage proliferation of HT-29 was significantly inhibited in dose-time dependent manner at 10 µM, 20 µM, 40 µM and 50 µM by DZ-BAU2021-14 after 48h (80 ± 5%, 68 ± 4%, 52 ± 2% and 48 ± 2%) and after 72h (67 ± 4%, 53 ± 9%, 40 ± 9%, and 34 ± 6%) respectively with an IC50 of 19 µM. In contrast, the percentage proliferation of HT-29 was significantly inhibited by DZ-BAU2021-14N at 50 µM after 24h (69 ± 10%) and at 40 µM after 72h (64 ± 4%) with an IC50 of 40 µM (Table 3) (Fig. 9). In this context, it is necessary to report that DZ-BAU2021-14N didn't reveal any advantage over DZ-BAU2021-14, actually almost equal effects were observed at different concentrations for the first 24h, while HT-29 cell lines experienced more resistance towards DZ-BAU2021-14N starting from day two (Fig. 10). These facts demonstrate that heterogeneity in cancer cell lines may result in differential responses to drug treatment. Additionally, the involvement of functional ester carbonyl groups in hydrogen bonding with stabilizer polymers deprives the pyrazolopyridine, DZ-BAU2021-14, from some of its anchoring aids that might be pharmacophoric for its biological activity.

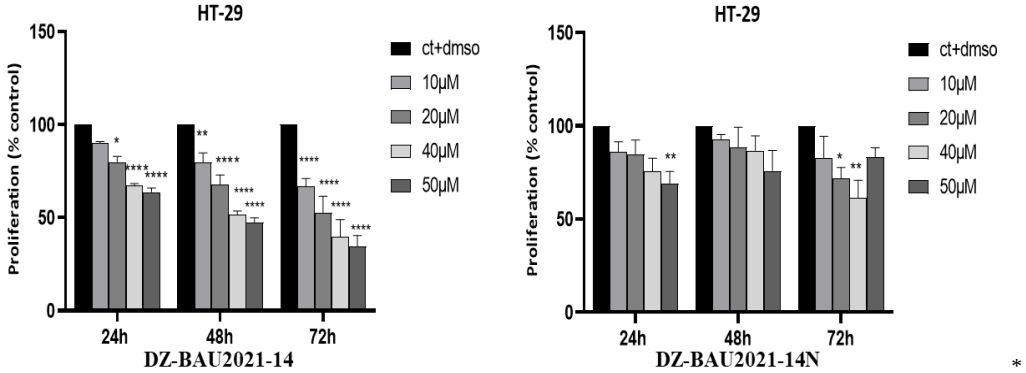

P<0.05, **0.01<P<0.05, ***P<0.001, ****P<0.0001, P-values were calculated in respect to DMSO

Fig.9: Percentage proliferation of HT-29 treated with DZ-BAU2021-14 and DZ-BAU2021-14N

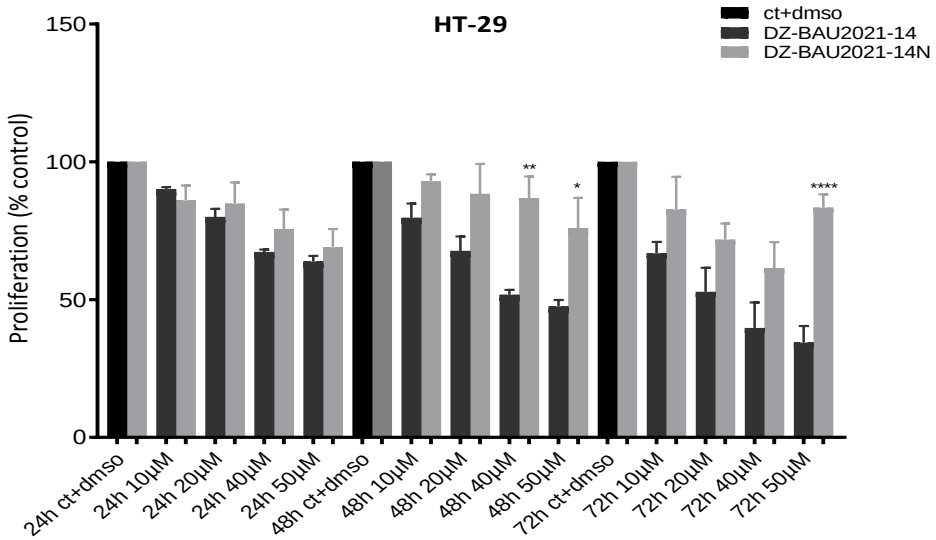

* P<0.05, **0.01<P<0.05, ***P<0.001, ****P<0.0001, P-values were calculated in respect to DZ-BAU2021-14

Fig.10: Comparative antiproliferative effect between DZ-BAU2021-14 and DZ-BAU2021-14N on HT-29

3.2.3. Antiproliferative effect on NCM-460D

Comparing cytotoxic potential of DZ-BAU2021-14 and DZ-BAU2021-14N on normal cell lines NCM-460D, the normal cells showed resistance towards the pharmaceutically untreated DZ-BAU2021-14 that demonstrated slight inhibition of percentage proliferation ranging between 9% and 23% at 48h and 72h for 40 µM and 50 µM with an IC50 value of 200 µM (Fig. 11). The fact that ensures a safety profile covering the antiproliferative effect of DZ-BAU2021-14. On the other hand, unfortunately DZ-BAU2021-14N has shown lower safety profile exhibiting significant inhibitory effect in a dose-time dependent manner at 10 µM, 20 µM, 40 µM and 50 µM after 48h and 72h on NCM-460D with an IC50 value of 33 µM (Table 4) (Fig. 12).

Table 4: Percentage proliferation of NCM-460D treated with DZ-BAU2021-14 and DZ-BAU2021-14N

Compound	**NCM-460D**								
	10 µM		**20 µM**		**40 µM**		**50 µM**		
	48 h	**72 h**	**48 h**	**72 h**	**48 h**	**72 h**	**48 h**	**72 h**	**IC50[2]**
DZ-BAU2021-14	107	111	103	100	91	90	85	78	200
St d[1]	17	19	12	9	20	28	14	22	
DZ-BAU2021-14N	83	59	73	57	53	42	60	38	33
St d[1]	17	12	10	26	4	8	11	8	

[1]Standard deviations are related to three separate experiments
[2]IC50 calculated after 72 h exposure to three separate experiments

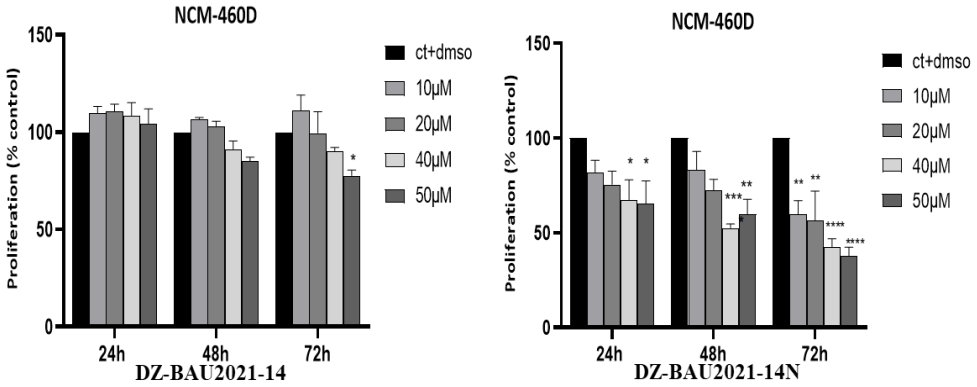

* P<0.05, **0.01<P<0.05, ***P<0.001, ****P<0.0001, P-values were calculated in respect to DMSO

Fig.11: Percentage proliferation of NCM-460D treated with DZ-BAU2021-14 and DZ-BAU2021-14N

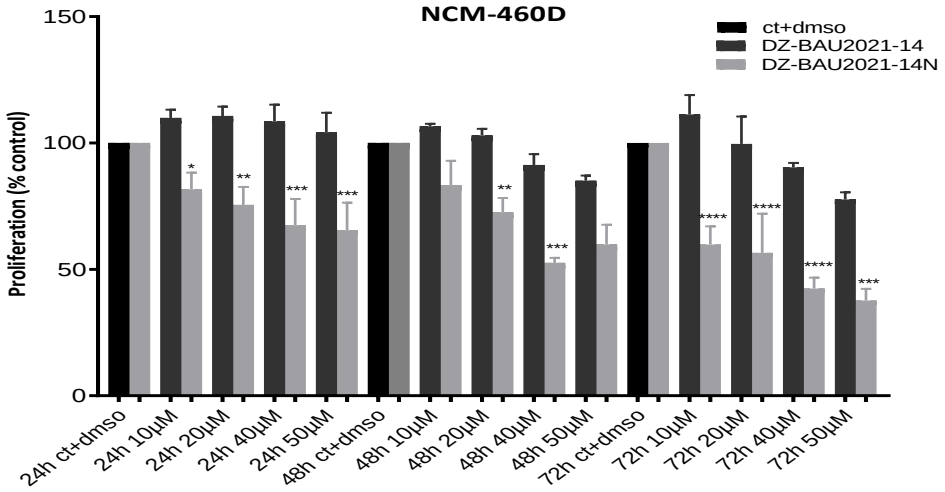

* P<0.05, **0.01<P<0.05, ***P<0.001, ****P<0.0001, P-values were calculated in respect to DZ-BAU2021-14

Fig.12: Comparative antiproliferative effect between DZ-BAU2021-14 and DZ-BAU2021-14N on NCM-460D

The obtained unanticipated results for the Nanocrystals DZ-BAU2021-14N towards different cell lines; namely the unsteady decreased antiproliferative effect on HT-29 and the increased cytotoxic on normal CRC, NCM-460D, can be related to abundant sets of possible explanations including permeability, transportation method, diffusion, integrity of cell membranes and others. In this respect, trying to find probable justification for different cellular responses towards the hydrophilic Nano formulation, the authors reviewed the colon adenoma carcinoma sequence. It was reported associated with alteration in cellular components one of which is lipid profile and lipid metabolism. Deregulation of lipid profile affects the synthesis of phospholipid cell membrane. This deregulation differs with individual variations and particular stages of CRC development (Hofmanová *et al.*, 2020). This precipitates heterogeneity between cell lines and hence affects both structure and function of cellular phospholipid membranes resulting in different behaviors and responses including morphology, permeability, and uptake. The unexpected not satisfying finding will not limit the researchers but will create an expanded margin for more investigations to achieve safety on NCM-460D cell lines.

4. CONCLUSION

In the frame of applying pharmaceutical sciences in an interdisciplinary approach, the promising DZ-BAU2021-14 was incorporated in a stable nanocrystalline formulation aiming at enhancing its antiproliferative effect and minimizing its cytotoxic effect. The free drug and its nanoformulation were comparatively evaluated for their *in-vitro* anticancer activity. DZ-BAU2021-14 was proved to inhibit cell growth of both colorectal cancer cell lines HT-29 and HCT-116. HT-29 was more sensitive towards DZ-BAU2021-14 compared to HCT-116, additionally, DZ-BAU2021-14 was non-cytotoxic on normal cell line NCM-460D with only a slight inhibition at late time point and high concentration. DZ-BAU2021-14N exhibited higher percentages inhibition against HCT-116 compared to HT-29 cells that were more resistant. On the other hand, DZ-BAU2021-14N affected NCM-460D at different concentrations and different time points. DZ-BAU2021-14 and DZ-BAU2021-14N generally showed minor differences on both colorectal cancer cell lines indicating that DZ-BAU2021-14N offered non statistically significant advantage over the parental molecule DZ-BAU2021-14. Although there was a non-statistically significant difference between DZ-BAU2021-14N and the parental molecule, yet the nanoformulation improved water solubility for the drug and provided more specificity toward HCT-116 cell line. The drawback of compound nanocrystal cytotoxicity will be considered a challenge that requires further investigations and studies.

5. ACKNOWLEDGMENT

The authors are thankful to Rayyan Boukarroum for conducting XRD study.

6. CONFLICT OF INTEREST

Authors declare no conflict of interest

REFERENCES

- Abaza, M. S., Bahman, A. M., & Al-Attiyah, R. J. (2008). Roscovitine synergizes with conventional chemo-therapeutic drugs to induce efficient apoptosis of human colorectal cancer cells. *World J Gastroenterol, 14*(33), 5162-5175.
- Abdelmohsen, S. A., & El Emary, T. I. (2014). Synthesis, characterization and antimicrobial activity of novel pyrazolo[3,4-b]pyridines and their spiro-heterocyclic derivatives. *Journal of Advances in Chemistry, 10*(7), 2901-2915.
- Aguayo, M. G., Fernández Pérez, A., Reyes, G., Oviedo, C., Gacitúa, W., Gonzalez, R., & Uyarte, O. (2018). Isolation and Characterization of Cellulose Nanocrystals from Rejected Fibers Originated in the Kraft Pulping Process. *Polymers (Basel), 10*(10).
- Alexis, F., Rhee, J. W., Richie, J. P., Radovic-Moreno, A. F., Langer, R., & Farokhzad, O. C. (2008). New frontiers in nanotechnology for cancer treatment. *Urol Oncol, 26*(1), 74-85.
- Alfarouk, K. O., Stock, C. M., Taylor, S., Walsh, M., Muddathir, A. K., Verduzco, D., Bashir, A. H., Mohammed, O. Y., Elhassan, G. O., et al. (2015). Resistance to cancer chemotherapy: failure in drug response from ADME to P-gp. *Cancer Cell Int, 15*, 71-83.

- Avari, R. B., S.; Mehrparvar, S.; Darvish, F.; Rominger, F.; Hamdan, F.; Mirzaie, S. Beilstein (2019). Efficient synthesis of pyrazolopyridines containing a chromane backbone through domino reaction. *J. Org. Chem, 15*, 874-880.
- Cicenas, J., Kalyan, K., Sorokinas, A., Stankunas, E., Levy, J., Meskinyte, I., Stankevicius, V., Kaupinis, A., & Valius, M. (2015). Roscovitine in cancer and other diseases. *Annals of translational medicine, 3*(10), 135-135.
- de Waard, H., Frijlink, H. W., & Hinrichs, W. L. (2011). Bottom-up preparation techniques for nanocrystals of lipophilic drugs. *Pharmaceutical research, 28*(5), 1220-1223.
- Dennis Bilavendran, J., Manikandan, A., Thangarasu, P., & Sivakumar, K. (2020). Synthesis and discovery of pyrazolo-pyridine analogs as inflammation medications through pro- and anti-inflammatory cytokine and COX-2 inhibition assessments. *Bioorganic Chemistry, 94*, 103484.
- El-Gohary, N. S., Hawas, S. S., Gabr, M. T., Shaaban, M. I., & El-Ashmawy, M. B. (2019). New series of fused pyrazolopyridines: Synthesis, molecular modeling, antimicrobial, antiquorum-sensing and antitumor activities. *Bioorganic Chemistry, 92*, 103109.
- Fares, J., Fares, M. Y., Khachfe, H. H., Salhab, H. A., & Fares, Y. (2020). Molecular principles of metastasis: a hallmark of cancer revisited. *Signal Transduction and Targeted Therapy, 5*(1), 28.
- Freag, M. S., Elnaggar, Y. S., & Abdallah, O. Y. (2013). Development of novel polymer-stabilized diosmin nanosuspensions: in vitro appraisal and ex vivo permeation. *Int J Pharm, 454*(1), 462-471. doi:10.1016/j.ijpharm.2013.06.039
- Hassan, A. S., Mady, M. F., Awad, H. M., & Hafez, T. S. (2017). Synthesis and antitumor activity of some new pyrazolo[1,5-a]pyrimidines. *Chinese Chemical Letters, 28*(2), 388-393.
- Hofmanová, J., Slavík, J., Ovesná, P., Tylichová, Z., Dušek, L., Straková, N., Vaculová, A. H., Ciganek, M., Kala, Z., et al. (2020). Phospholipid profiling enables to discriminate tumor- and non-tumor-derived human colon epithelial cells: Phospholipidome similarities and differences in colon cancer cell lines and in patient-derived cell samples. *PloS one, 15*(1), e0228010.
- Hu, X., Wan, B., Liu, Y., Shen, J., Franzblau, S. G., Zhang, T., Ding, K., & Lu, X. (2019). Identification of Pyrazolo[1,5-a]pyridine-3-carboxamide Diaryl Derivatives as Drug Resistant Antituberculosis Agents. *ACS Medicinal Chemistry Letters, 10*(3), 295-299.
- Ismail, N. S. M., Ali, E. M. H., Ibrahim, D. A., Serya, R. A. T., & Abou El Ella, D. A. (2016). Pyrazolo[3,4-d]pyrimidine based scaffold derivatives targeting kinases as anticancer agents. *Future Journal of Pharmaceutical Sciences, 2*(1), 20-30.
- Jemal, A., Ward, E. M., Johnson, C. J., Cronin, K. A., Ma, J., Ryerson, B., Mariotto, A., Lake, A. J., Wilson, R., et al. (2017). Annual Report to the Nation on the Status of Cancer, 1975-2014, Featuring Survival. *J Natl Cancer Inst, 109*(9).
- Kamel, A. O., Awad, G. A. S., Geneidi, A. S., & Mortada, N. D. (2009). Preparation of intravenous stealthy acyclovir nanoparticles with increased mean residence time. *AAPS PharmSciTech, 10*(4), 1427-1436.
- Karrouchi, K., Radi, S., Ramli, Y., Taoufik, J., Mabkhot, Y. N., Al-Aizari, F. A., & Ansar, M. h. (2018). Synthesis and Pharmacological Activities of Pyrazole Derivatives: A Review. *Molecules (Basel, Switzerland), 23*(1), 134-219.
- Kassem, Z., Abou Merhi, R., & Issa, D. (2020). Discovery of pyrazolopyridine derivatives dually targeting inflammation and proliferation in colorectal cancer cell lines: In-silico drug design approach. *BAU Journal - Health and Wellbeing, 4*(1), 1-12. Retrieved from https://digitalcommons.bau.edu.lb/hwbjournal/vol4/iss1/1
- Kassem, Z. A., Abou Staiteieh, S., Nasr, J., Youssef, A., Darwish, N., Borjac, J., Abou Merhi, R., & Issa, D. A. E. (2021). Design, synthesis of novel pyrazolo[3,4-b]pyridine derivatives and evaluation of their antiproliferative effect as Cyclin Dependent Kinase 2 (CDK2) inhibitors *Under publication*.
- Kaviyarasu, K., Murmu, P. P., Kennedy, J., Thema, F. T., Letsholathebe, D., Kotsedi, L., & Maaza, M. (2017). Structural, optical and magnetic investigation of Gd implanted CeO2 nanocrystals. *Nuclear Instruments and Methods in Physics Research Section B: Beam Interactions with Materials and Atoms, 409*, 147-152.
- Kuipers, E. J., Grady, W. M., Lieberman, D., Seufferlein, T., Sung, J. J., Boelens, P. G., van de Velde, C. J. H., & Watanabe, T. (2015). Colorectal cancer. *Nature reviews. Disease primers, 1*, 15065-15065.
- Kumar Shital. (2021). New Ideas in Cancer Treatment,. Retrieved from https://www.webmd.com/cancer/cancer-new-research-treatment
- Lin, R., Connolly, Peter J., Lu, Yanhua, Chiu, George ,Li, Shengjian, Yu, Y., Huang, Shenlin, Li, Xun, Emanuel, Stuart L., Middleton, Steven A., Gruninger, R. H., Adams, Mary, Fuentes-Pesquera, Angel

R., & Greenberger, L. M. (2007). Synthesis and evaluation of pyrazolo[3,4-b]pyridine CDK1 inhibitors as anti-tumor agents. *Bioorganic & Medicinal Chemistry Letters, 17*(15), 4297-4302.

- Madheswaran, T., Baskaran, R., Yong, C. S., & Yoo, B. K. (2014). Enhanced topical delivery of finasteride using glyceryl monooleate-based liquid crystalline nanoparticles stabilized by cremophor surfactants. *AAPS PharmSciTech, 15*(1), 44-51.
- McClue, S., Blake, D., Clarke, R., Cowan, A., Cummings, L., Fischer, P., MacKenzie, M., Melville, J., Stewart, K., et al. (2002). In vitro and in vivo antitumor properties of the cyclin dependent kinase inhibitor CYC202 (R-roscovitine). *International journal of cancer. Journal international du cancer, 102*, 463-468.
- Mehanna, M. M., Mneimneh, A. T., & Abed El Jalil, K. (2020). Levofloxacin-loaded naturally occurring monoterpene-based nanoemulgel: a feasible efficient system to circumvent MRSA ocular infections. *Drug Dev Ind Pharm, 46*(11), 1787-1799.
- Mohyeldin, S. M., Mehanna, M. M., & Elgindy, N. A. (2016). The relevancy of controlled nanocrystallization on rifampicin characteristics and cytotoxicity. *International journal of nanomedicine, 11*, 2209-2222.
- Pick, A., Klinkhammer, W., & Wiese, M. (2010). Specific inhibitors of the breast cancer resistance protein (BCRP). *ChemMedChem, 5*(9), 1498-1505.
- Pinheiro, L., Feitosa, L., Gandi, M., Silveira, F., & Boechat, N. (2019). The Development of Novel Compounds Against Malaria: Quinolines, Triazolpyridines, Pyrazolopyridines and Pyrazolopyrimidines. *Molecules, 24*, 4095.
- Rajendra, A., Ariane, R., Philip Michael, H., Michael John, R., Kamal, D., & Mary, B. (2018). Nanoparticles in Cancer Treatment: Opportunities and Obstacles. *Current Drug Targets, 19*(14), 1696-1709.
- Reinecke, P., Corvin, J., Gabbert, H. E., & Gerharz, C. D. (1997). Antiproliferative effects of paclitaxel (Taxol®) on human renal clear cell carcinomas in vitro. *European Journal of Cancer, 33*(7), 1122-1129.
- Rejhová, A., Opattová, A., Čumová, A., Slíva, D., & Vodička, P. (2018). Natural compounds and combination therapy in colorectal cancer treatment. *Eur J Med Chem, 144*, 582-594.
- Saindane, N. S., Pagar, K. P., & Vavia, P. R. (2013). Nanosuspension based in situ gelling nasal spray of carvedilol: development, in vitro and in vivo characterization. *AAPS PharmSciTech, 14*(1), 189-199.
- Siegel, R. L., Miller, K. D., & Jemal, A. (2019). Cancer statistics, 2019. *CA Cancer J Clin, 69*(1), 7-34.
- Stintzing, S., Tejpar, S., Gibbs, P., Thiebach, L., & Lenz, H. J. (2017). Understanding the role of primary tumour localisation in colorectal cancer treatment and outcomes. *Eur J Cancer, 84*, 69-80.
- Subhashni D. Singh-Joy, V. C. M. (2008). Safety Assessment of Poloxamers 101, 105, 108, 122, 123, 124, 181, 182, 183, 184, 185, 188, 212, 215, 217, 231, 234, 235, 237, 238, 282, 284, 288, 331, 333, 334, 335, 338, 401, 402, 403, and 407, Poloxamer 105 Benzoate, and Poloxamer 182 Dibenzoate as Used in Cosmetics. [Reviewed by the Cosmetic Ingredient Review (CIR) Expert Panel]. *International Journal of Toxicology, 27*(2_suppl), 93-128.
- Taha, H., Mohamed, S. H., & Hassan, Z. (2020). Evaluation of roscovitine anticancer agent as a reference compound for cancer and apoptosis studies. *Journal of Innovations in Pharmaceutical and Biological Sciences 6*, 53-56. Retrieved from www.researchgate.net
- Tian, X., Li, H., Zhang, D., Liu, G., Jia, L., Zheng, D., Shen, J., Shen, Y., & Zhang, Q. (2013). Nanosuspension for parenteral delivery of a p-terphenyl derivative: Preparation, characteristics and pharmacokinetic studies. *Colloids and Surfaces B: Biointerfaces, 108*, 29-33.
- Zhou, X., Zhu, X., Wang, B., Li, J., Liu, Q., Gao, X., Sirkar, K. K., & Chen, D. (2018). Continuous production of drug nanocrystals by porous hollow fiber-based anti-solvent crystallization. *Journal of Membrane Science, 564*, 682-690.